Research article

Dongyang Wang, Changxu Liu, Shuang Zhang* and Che Ting Chan*

Chaotic photon spheres in non-Euclidean billiard

https://doi.org/10.1515/nanoph-2020-0083
Received February 3, 2020; accepted April 1, 2020; published online May 14, 2020

Abstract: With the advancement in understanding of the physics inside chaotic systems, chaos has been harnessed from a nuisance to a beneficial factor in optical devices. Light–matter interaction in chaotic systems has been utilised for improving broadband energy harvesting and momentum transformations, achieving light localization beyond diffraction limit and even stabilizing the dynamics of high power laser. While extensive study about wave chaos has been made in deformed microcavities, investigation of how chaos dynamics evolves in curved space manifold remains elusive. Here, we study the non-Euclidean billiard of a torus-like manifold, which is a closed 2D cavity system with effective periodic boundaries. The ray chaotic behaviours on the deformed toroidal surface are explored using the geodesic equation. By tuning the deformation parameter of the torus, we observe the transition of the billiard from the ordered phase state to mixed phase states and then complete ray chaos. The photon sphere of the torus is identified as the transition position from ordered states to chaotic states. Compared with other chaotic behaviours resulted from the random scattering inside deformed cavities, we demonstrate chaotic dynamics purely on a curved surface, which may shed light on the better understanding of chaos in optics.

Keywords: chaos; deformation; manifold; non-Euclidean billiard; toroidal surface.

Current address: Changxu Liu, Chair in Hybrid Nanosystems, Nanoinstitute Munich, Faculty of Physics, Ludwig Maximilians, University of Munich, Munich, 80539, Germany.

***Corresponding authors: Shuang Zhang**, School of Physics & Astronomy, University of Birmingham, Birmingham, B15 2TT, UK, E-mail: s.zhang@bham.ac.uk; and **Che Ting Chan**, Department of Physics, Hong Kong University of Science and Technology, Hong Kong, PR China, E-mail: phchan@ust.hk

Dongyang Wang: Department of Physics, Hong Kong University of Science and Technology, Hong Kong, PR China. https://orcid.org/0000-0002-6969-2354

Changxu Liu: School of Physics & Astronomy, University of Birmingham, Birmingham, B15 2TT, UK

Chaos is a ubiquitous phenomenon in Nature, ranging from celestial mechanism, climate change, population evolution to chemical reactions and biological homoeostasis [1]. Since the study of three-body problem by Henri Poincare, chaos has been extensively studied in many systems, ranging from electronics to fluids, brains and more recently photonics [2, 3]. Due to the exponential sensitivity to initial conditions, the output of a chaotic system is unpredictable, and chaotic response has been considered as a nuisance in scientific systems. However, a deeper understanding of the physics of chaos can turn it into a beneficial factor. Particularly in optics, chaos is harnessed and utilized for a repertoire of applications, including broadband energy harvesting [4], light localization beyond diffraction limit [5], realizing superradiance [6], stabilizing high-power lasers [7] and broadband momentum transformations [8].

Among various optical systems, deformed microcavities provide a feasible platform to investigate multiple areas of physics including lasing modulation [9–19], nonlinear dynamics [20–23], non-Hermitian physics [24–31], and quantum chaos [32–38]. Microcavity is also a model system to study the quantum correspondence of classical chaos, due to the formal analogy between the Schrodinger equation and the Maxwell equation. As such, the chaotic behaviour of classical billiards such as dielectric plates or disks [31, 36–38] are widely studied.

Although optical cavities with different shapes [12, 13, 39–45] and different kinds of boundary deformation have been studied [6, 15, 46, 47], the chaotic behaviour in curved space manifold has not been explored yet. Inspired by general relativity, curved space provides a conceptual new pathway to manipulate the trajectory of light [48–51]. A detailed study of the chaotic dynamics in the novel system is of crucial importance in both fundamental physics and practical applications. More importantly, curvature-induced dynamics of electromagnetics mainly occurs on the surface, differentiating itself from scattering-based cases inside a cavity. Here, we consider a non-Euclidean billiard and study the chaotic features of the geometrical optics on a toroidal 2D manifold with analogical quadrupolar deformation [38]. For the curved space geometry, we consider a relatively large-scale model system where wave properties are less predominant, thus the short wavelength limit is taken and we study the ray chaotic

phenomena for a toroidal surface by tracing the ray trajectories.

For an un-deformed torus, the existence of rotation symmetry guarantees an additional constant of motion, which is the angular momentum about the centre axis, and chaotic features are prohibited. However, chaos can emerge if the torus is deformed. We introduce the widely adopted quadrupolar deformation to the torus parameterization as

$$\begin{aligned} x &= (R_0 + r_0\cos\theta)(1 + e\cos 2\varphi)\cos\varphi \\ y &= (R_0 + r_0\cos\theta)(1 + e\cos 2\varphi)\sin\varphi \\ z &= r_0(1 + e\cos 2\varphi)\sin\theta \end{aligned}$$

where e is the deformation size parameter. The torus parameters are shown in Figure 1a, and the deformation is illustrated schematically in Figure 1b.

Chaotic behaviours can usually be shown as phase space trajectories, using position and momentum as coordinates. For the dynamical billiard system, the position and incident angle onto the boundaries are usually adopted as the phase space coordinated pair. For the case of our toroidal manifold shown in Figure 1a and b, an analogy is taken and we define $(\varphi, \cos\chi)$ as the Birkhoff coordinates in phase space, where φ is the angular position of rays coming across the outer equator, and χ is the propagation angle with respect to the outer equator at the position φ (propagation angle χ is more clearly defined in Supplementary Information 1), the phase space coordinates are indicated pictorially in Figure 1a.

The ray trajectories on the deformed toroidal surface can be determinately calculated using the geodesic equation (as derived in Supplementary Information 2), where the travelling route is fully deterministic once the initial conditions of position and propagation direction are specified. The phase space information can be extracted from the ray trajectories. When deformation is introduced, we first calculate the phase diagram with the Birkhoff coordinates defined above. The results are shown in Figure 1c–f, where a series of deformation values e are considered, and the excitation source is set at the position of $\varphi = 0$, $\theta = 0$ on the outer equator. As can be seen from Figure 1c, for the case of $e = 0$ where the torus is not deformed, ray trajectories are straight line segment in phase space, which clearly shows an ordered state. When the deformation is gradually increased as shown in Figure 1d, trajectories corresponding to lower and higher values of $\cos\chi$ becomes curvy, which are still ordered states. But the trajectories become totally disordered at the centre part where $\cos\chi \sim 0.5$, representing the chaotic states of deformed torus, and the system can thus be identified as in a mixed chaotic state. As the deformation further increases as shown in Figure 1e and f, the chaotic region expands towards the higher and lower boundaries of $\cos\chi$, and the mixed state gradually approach a fully chaotic state.

It can be seen that the chaotic regions in Figure 1d–f are centred around $\cos\chi = 0.5$, which is the critical propagation condition shown in Figure 2a that separates free rays (twisting around the torus along θ direction for rays with $\cos\chi > 0.5$) and reflected rays (turning back at some critical position of $\theta = \theta_c$ for rays with $\cos\chi < 0.5$) on a torus manifold, as discussed in a previous study [51]. This particular propagation angle corresponds to the peculiar ray with real space trajectory shown in panel (a). This trajectory has an extremely long occupation time near the

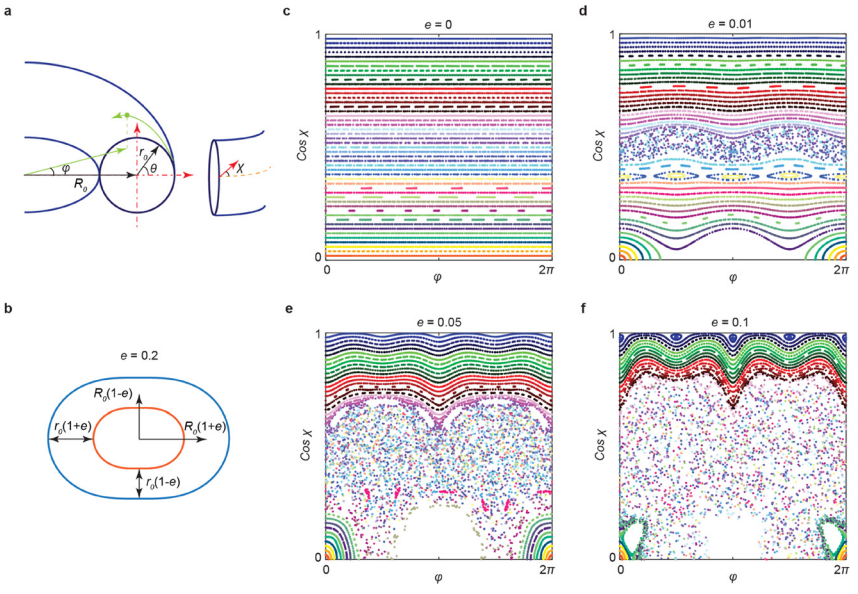

Figure 1: Schematics of the deformed toroidal manifold and the chaotic transition of the billiard. (a) Parametrization of the toroidal surface. (b) Schematics illustrating the toroidal inner and outer equators with a quadrupolar deformation, parameterized by deformation size parameter "e". (c) Phase space diagram with no deformation. (d-f) Phase space diagrams when $e = 0.01$, 0.05, 0.1, respectively. The geometrical parameter is set as a = $r_0/R_0 = 1/3$.

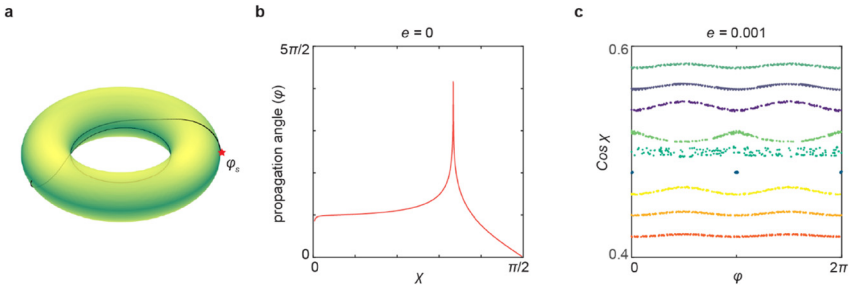

Figure 2: Ray propagation and chaotic trajectories near the photon sphere. (a) Ray tracing near the photon sphere for the undeformed torus. The red star marks the position of the source. (b) Calculated propagation angle φ traversed by the rays before coming back to outer equator for different propagation angles χ between 0 and $\pi/2$ for an undeformed torus. The peak at $\chi = \pi/3$ defines the photon sphere. (c) Chaotic trajectories for a very small deformation of $e = 0.001$, the chaotic behaviour can be traced to start from the photon sphere position.

inner equator of an undeformed torus as shown in Figure 2b, where the propagated φ angles traversed by the rays (proportional to the propagation lifetime) before going back to outer equator are plotted as the y-axis. The ray trajectory near the inner equator is similar to the photon sphere in the case of black hole imitation with metamaterials where rays are trapped inside the metamaterial [52]. We further reduce the deformation scale to a small value of $e = 0.001$ to track the onset of chaotic behaviour as shown in Figure 2c. We see that the emergence of phase space disorder can be traced to start from the photon sphere position. The particular ray can thus be addressed as the chaotic photon sphere that separate ordered and chaotic phases of the deformed toroidal billiard.

We note that different shapes of trajectories show up in the phase diagram. By tracing the corresponding ray trajectories in real space, we can examine the connection between real space propagation and phase space manifestation. Several propagation angles are chosen from Figure 1e, and the traced trajectories are shown in Figure 3 for both manifold and parameter space presentation. The trajectories for small values of angle χ are shown in Figure 3a and d. The rays are confined along the θ direction within the region near the outer equator, which are the reflected-type rays and correspond to the curly lines in phase space at the upper part of Figure 1e. In Figure 3b and e, we consider a value of χ located in the chaotic region, and the confinement ceases to be effective and rays goes through the manifold freely. As the angle further increases and go beyond the chaotic region, the rays are again confined as shown in Figure 3c and f. However, the confinement is now along the φ direction, which is caused by the curvature difference at different φ positions. The manifestation of this ray trajectory in phase space is a half-closed circle in lower part of Figure 1e. It is worth to note that for the special condition of ray trajectories being closed, the Birkhoff coordinates will show up as islands in phase diagram, as can be found from Figure 1d–f.

The existence of two different kinds of confinement stems from the curvature change at different positions and can be more intuitively explained as a consequence of angular momentum conservation using configurations

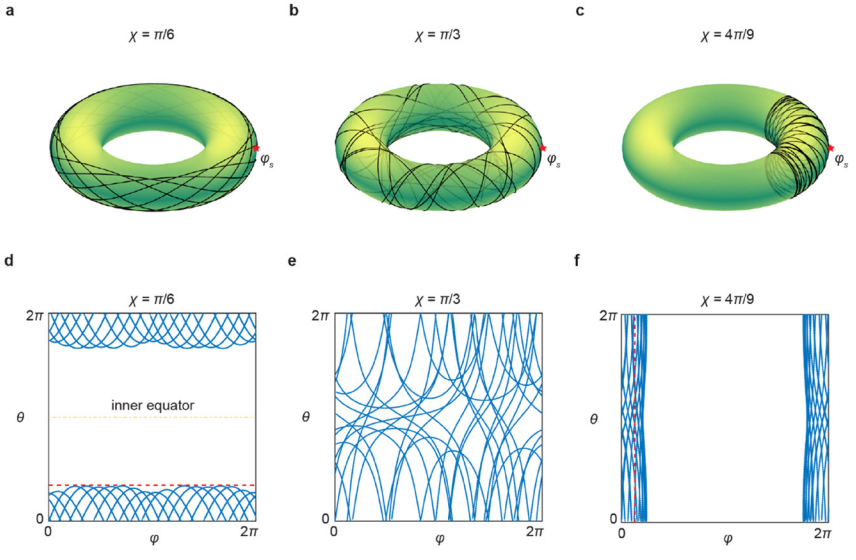

Figure 3: Real space manifestation of the trajectories in phase diagram. The upper panels show ray trajectories in real space and the lower panels show corresponding trajectories in parameter space. (a) Confined rays in θ direction for a propagation angle of $\chi = \pi/6$, corresponding to the curly lines in phase diagram. (b) Ray trajectory for a larger propagation angle of $\chi = \pi/3$, corresponding to chaotic dots in phase diagram. (c) Confined ray in φ direction for propagation angle of $\chi = 4\pi/9$, corresponding to the curly circle in phase diagram. (d-f) parameters space presentation of ray trajectories in (a-c) The predicted confined positions (see Supplementary Information 2) are plotted with red dashed lines in (d) and (f). The deformation parameter is taken as $e = 0.05$ for all conditions of (a-c) and the excitation source positions φ_s are marked as red stars.

with certain restored symmetry. We consider two configurations as shown in Figure 4a and b, respectively. The standard torus with no deformation is considered in Figure 4a, where the conservation of angular momentum about the torus centre axis direction gives the following relationship of critical travelling position:

$$R_c = R_s \cos\chi$$

with R_s being the projected radius value of source position onto the inner and outer equators plane, which gives the critical θ value of for ray propagation as:

$$\theta = \cos^{-1}\frac{R_s \cos\chi - R_0}{r_0}$$

The critical θ value for propagations from outer equator ($Rs = R_0 + r_0$) with different incident angles are shown in Figure 4c, where the propagation initial condition of $\chi = \pi/6$ (case of Figure 3a and d) is marked as red circle. In Figure 4b, a conus is considered to account for the radius change along the φ direction in the deformed torus. By neglecting the torus bending along the equator direction, the angular momentum of conus about the centre axis is conserved, and we have the following equation of critical travelling position:

$$r_c = r_s \sin\chi$$

with r_s being the radius of conus at the source position and the critical φ value of ray propagation can be calculated as

$$\varphi_c = \frac{1}{2}\cos^{-1}\left(\frac{r_s \sin\chi}{e r_0} - \frac{1}{e}\right)$$

the propagation angle dependence of critical angle is shown in Figure 4d. The condition of $\chi = 4\pi/9$ (case of Figure 3c and f) is marked as red circle. The prediction in Figure 4d is less accurate (as indicated by the red line in Figure 3f) due to the severe bending of the tube being ignored.

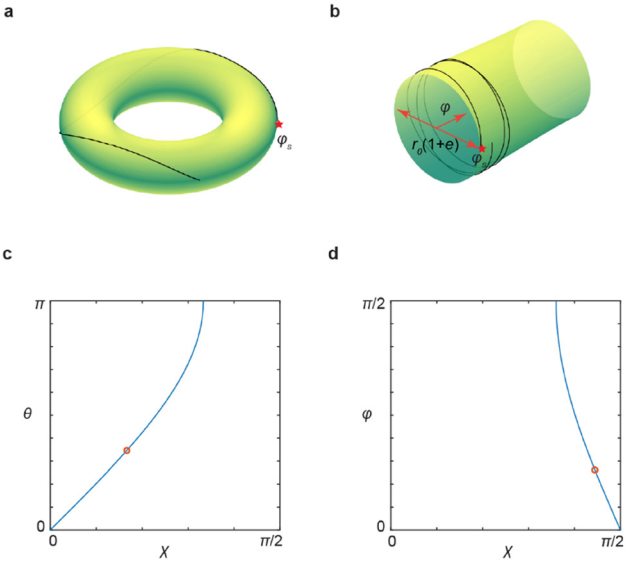

Figure 4: The critical reflection with restored symmetry for different propagation angles. (a) Undeformed torus for θ confinement. The source position φ_s is marked by a red star. (b) Conus surface to explain the φ confinement. Source position φ_s is marked by a red star. (c) Critical reflection positions of the torus for different initial propagation angles. The coordinates for position marked by the red circle are $(\chi, \theta) = (\pi/6, 0.3464\pi)$ corresponding to the dashed line in Figure 3d. (d) Critical reflection positions of conus for different initial propagation angles, where conus is defined as $r = r_0\,(1 + e\cos 2\varphi)$, $x = r\cos\theta, y = r\cos\theta, z = r_0/a\,\varphi$. The coordinates for position marked by red circle are $(\chi, \varphi) = (4\pi/9, 0.1308\pi)$, corresponding to the dashed line in Figure 3f.

The two types of confinement along φ and θ directions, respectively, are related to the two types of photon spheres. One of which is located near the inner equator as the case of Figure 3a and d, which is the property of an undeformed torus. The other one is induced by deformation and located at the cylindrical cross section of torus. In order to locate the photon sphere, a geometrical ray tracing is considered where both the position of the ray source φ_s on the outer equator and direction of ray propagation angle χ are scanned. By calculating the φ and θ distance traversed by ray trajectories before going back to the outer equator, which is an effective lifetime, the two types of photon sphere can each be identified by the long φ occupation or θ occupation times, respectively. In Figure 5a, we consider the case of no deformation and the first type photon sphere (long φ occupation) coincide with the inner equator of the torus. When the deformation is applied to the torus, the shape of the first type photon sphere will deviate from a standard circle as shown in Figure 5b, where a deformation scale of $e = 0.05$ is adopted. In Figure 5c, the traced θ-lifetime distributions are shown, where the long lifetime positions can be found at the right side corresponding to the deformation induced photon sphere. It is worth to note that, due to the absence of rotation symmetry, the photon sphere depends on the source position along θ direction as well, and can be further tuned by deformation scale factor. These details are discussed in Supplementary Information 3.

In conclusion, we have studied the chaotic behaviour of rays travelling on a 2D manifold with a toroidal-like deformed surface, where the onset of chaos was found to emerge from the photon sphere of the torus. By tuning the

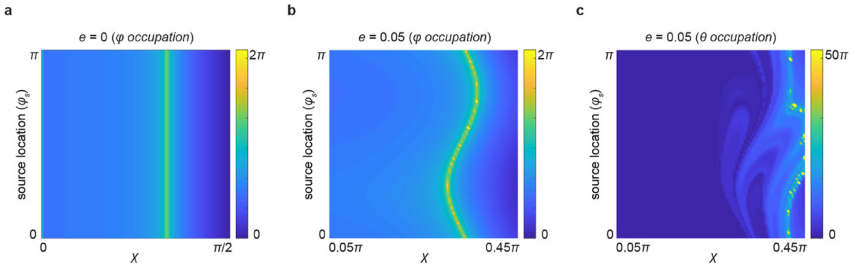

Figure 5: Deformation of the photon sphere with respect to deformation parameter e. (a) Photon sphere of the undeformed torus with $e = 0$. (b) Photon sphere evolution with the excitation source located at different φ position around the outer equator, colour intensity stands for the total propagation angle φ the ray traversed before going back to the outer equator, and the deformation parameter is $e = 0.05$. (c) Evolution of deformation induced photon sphere that confines rays along φ direction, the excitation source is considered to be located at different φ position around the outer equator, colour stands for the propagation θ angle when rays go back to outer equator, and the deformation parameter is $e = 0.05$.

deformation parameter, the non-Euclidean billiard goes from an ordered state to mixed chaotic states and then nearly full chaos at large deformation. Two kinds of confinement are also found for the deformed toroidal billiard, which corresponds to different trajectories in the phase space diagram. This provides a complement for chaos induced by random scattering inside deformed optical cavities, demonstrating an alternative way to achieve chaotic dynamics purely on a surface with curvature engineering.

The chaotic behaviour on toroidal surface we discovered could potentially be used in cavity design and leads to applications such as lasing modulation, nonlinear process control and energy harvesting. The path dependent response of the chaotic system could also be useful in optical communication. The phenomenon of curvature induced chaos can also be manifested in optical devices by nanostructure engineering, which will provide new function in photonic devices and integrated optical systems.

Acknowledgements: This work is supported by Research Grants Council (RGC) of Hong Kong by grants AoE/P-02/12 and 16303119.

References

[1] C. Letellier, 2011. *Chaos in Nature*. World Scientific.
[2] K. T. Alligood, T. Sauer, J. A. Yorke, 1996. *Chaos: An Introduction to Dynamical Systems*. Springer, New York.
[3] H.-J. Stöckmann, 1999. *Quantum Chaos: An Introduction*. Cambridge University Press, Cambridge.
[4] C. Liu, A. Di Falco, D. Molinari, et al., 2013. Enhanced energy storage in chaotic optical resonators. Nat. Photon. 7, 473–478. https://doi.org/10.1038/NPHOTON.2013.108.
[5] C. Liu, R. E. C. van der Wel, N. Rotenberg, et al., 2015. Triggering extreme events at the nanoscale in photonic seas. Nat. Phys. 11, 358–363. https://doi.org/10.1038/nphys3263.
[6]. C. Liu, A. Di Falco, and A. Fratalocchi, "Dicke phase transition with multiple superradiant states in quantum chaotic resonators," Phys. Rev. X, vol. 4, 2014, Art no. 021048, https://doi.org/10.1103/PhysRevX.4.021048.
[7] S. Bittner, S. Guazzotti, Y. Zeng, et al., 2018. Suppressing spatiotemporal lasing instabilities with wave-chaotic microcavities. Science 361, 1225. https://doi.org/10.1126/science.aas9437.
[8] X. Jiang, L. Shao, S.-X. Zhang, et al., 2017. Chaos-assisted broadband momentum transformation in optical microresonators. Science 358, 344. https://doi.org/10.1126/science.aao0763.
[9] J. U. Nöckel, A. D. Stone, R. K. Chang, 1994. Q spoiling and directionality in deformed ring cavities. Opt. Lett. 19, 1693–1695. https://doi.org/10.1364/OL.19.001693.
[10] J. U. Nöckel, A. D. Stone, G. Chen, H. L. Grossman, and R. K. Chang, "Directional emission from asymmetric resonant cavities," Opt. Lett. vol. 1921, pp. 1609–1611, 1996, https://doi.org/10.1364/ol.21.001609.
[11] C. Gmachl, F. Capasso, E. E. Narimanov, et al., 1998. High-power directional emission from microlasers with chaotic resonators. Science 280, 1556. https://doi.org/10.1126/science.280.5369.1556.
[12] G. D. Chern, H. E. Tureci, A. D. Stone, R. K. Chang, M. Kneissl, N. M. Johnson, 2003. Unidirectional lasing from InGaN multiple-quantum-well spiral-shaped micropillars. Appl. Phys. Lett. 83, 1710–1712. https://doi.org/10.1063/1.1605792.
[13] M.S. Kurdoglyan, S.-Y. Lee, S. Rim, C.-M. Kim, 2004. Unidirectional lasing from a microcavity with a rounded isosceles triangle shape. Opt. Lett. 1929, 2758–2760. https://doi.org/10.1364/OL.29.002758.
[14] J. Wiersig and M. Hentschel, "Combining directional light output and ultralow loss in deformed microdisks," Phys. Rev. Lett., vol. 100, 2008, Art no. 033901, https://doi.org/10.1103/PhysRevLett.100.033901.
[15] Q. Song, W. Fang, B. Liu, S.-T. Ho, G. S. Solomon, and H. Cao, "Chaotic microcavity laser with high quality factor and unidirectional output," Phys. Rev. A, vol. 80, 2009, Art no. 041807, https://doi.org/10.1103/PhysRevA.80.041807.
[16] C. Yan, Q. J. Wang, L. Diehl, et al., "Directional emission and universal far-field behavior from semiconductor lasers with limaçon-shaped microcavity," Appl. Phys. Lett., vol. 94, 2009, Art no. 251101, https://doi.org/10.1063/1.3153276.
[17] C.-H. Yi, M.-W. Kim, and C.-M. Kim, "Lasing characteristics of a Limaçon-shaped microcavity laser," Appl. Phys. Lett., vol. 95, 2009, Art no. 141107, https://doi.org/10.1063/1.3242014.
[18] S. Shinohara, M. Hentschel, J. Wiersig, T. Sasaki, and T. Harayama, "Ray-wave correspondence in limaifmmode mbox{c {c}}else c{c}fi{}on-shaped semiconductor microcavities," Phys. Rev. A, vol. 80, 2009, Art no. 031801, https://doi.org/10.1103/PhysRevA.80.031801.

[19] F. Albert, C. Hopfmann, A. Eberspächer, et al., "Directional whispering gallery mode emission from Limaçon-shaped electrically pumped quantum dot micropillar lasers," Appl. Phys. Lett., vol. 101, 2012, Art no. 021116, https://doi.org/10.1063/1.4733726.
[20] T. Harayama, T. Fukushima, S. Sunada, and K. S. Ikeda, "Asymmetric stationary lasing patterns in 2D symmetric microcavities," Phys. Rev. Lett., vol. 91, 2003, Art no. 073903, https://doi.org/10.1103/PhysRevLett.91.073903.
[21] T. Harayama, S. Sunada, and K. S. Ikeda, "Theory of two-dimensional microcavity lasers," Phys. Rev. A, vol. 72, 2005, Art no. 013803, https://doi.org/10.1103/PhysRevA.72.013803.
[22] T. Harayama, S. Shinohara, 2011. Two-dimensional microcavity lasers," Laser Photon. Rev. 5, 247–271. https://doi.org/10.1002/lpor.200900057.
[23] R. Leijssen, G. R. La Gala, L. Freisem, J. T. Muhonen, and E. Verhagen, "Nonlinear cavity optomechanics with nanomechanical thermal fluctuations," Nat. Commun., vol. 8, 2017, Art no. 16024, https://doi.org/10.1038/ncomms16024.
[24] W. D. Heiss, 1999. Phases of wave functions and level repulsion. Eur. Phys. J. D – Atom. Mol. Opt. Plasma Phys. 7, 1–4. https://doi.org/10.1007/s100530050339.
[25] W. D. Heiss, 2000. Repulsion of resonance states and exceptional points. Phys. Rev. E 61, 929–932. https://doi.org/10.1007/s100530050339.
[26] E. Persson, I. Rotter, H. J. Stöckmann, M. Barth, 2000. Observation of resonance trapping in an open microwave cavity. Phys. Rev. Lett. 85, 2478–2481. https://doi.org/10.1103/PhysRevLett.85.2478.
[27] C. Dembowski, H. D. Gräf, H. L. Harney, et al., 2001. Experimental observation of the topological structure of exceptional points. Phys. Rev. Lett. 86, 787–790. https://doi.org/10.1103/PhysRevLett.86.787.
[28] C. Dembowski, B. Dietz, H. D.Gräf, et al., "Encircling an exceptional point," Phys. Rev. E, vol. 69, 2004, Art no. 056216, https://doi.org/10.1103/PhysRevE.69.056216.
[29] S.-B. Lee, J. Yang, S. Moon, et al., "Observation of an exceptional point in a chaotic optical microcavity," Phys. Rev. Lett., vol. 103, 2009, Art no. 134101, https://doi.org/10.1103/PhysRevLett.103.134101.
[30] S.-Y. Lee, "Geometrical phase imprinted on eigenfunctions near an exceptional point," Phys. Rev. AArt, vol. 82no., 2010, 064101, https://doi.org/10.1103/PhysRevA.82.064101.
[31] H. Cao, J. Wiersig, 2015. Dielectric microcavities: model systems for wave chaos and non-Hermitian physics. Rev. Mod. Phy. 87, 61–111. https://doi.org/10.1103/RevModPhys.87.61.
[32] Davis, M.J., Heller, E.J., 1981. Quantum dynamical tunneling in bound states. J. Chem. Phys. 75, 246–254. https://doi.org/10.1063/1.441832.
[33] S. Fishman, D. R. Grempel, R. E. Prange, 1982. Chaos, quantum recurrences, and anderson localization. Phys. Rev. Lett. 49, 509–512. https://doi.org/10.1103/PhysRevLett.49.509.
[34] H. J. Stöckmann, J. Stein, 1990. 'Quantum' chaos in billiards studied by microwave absorption. Phys. Rev. Lett. 64, 2215–2218. https://doi.org/10.1103/PhysRevLett.64.2215.
[35] K. M. Frahm, D. L. Shepelyansky, 1997. Quantum localization in rough billiards. Phys. Rev. Lett. 78, 1440–1443. https://doi.org/10.1103/PhysRevLett.78.1440.
[36] J. U. Nöckel, A. D. Stone, 1997. Ray and wave chaos in asymmetric resonant optical cavities. Nature 385, 45–47. https://doi.org/10.1038/385045a0.
[37] A. D. Stone, 2001. Wave-chaotic optical resonators and lasers. Phys. Scr. T90, 248–262. https://doi.org/10.1088/0031-8949/2001/T90/036.
[38] H. E. Türeci, H. G. L. Schwefel, P. Jacquod, A. D. Stone, 2005. Chapter 2 – Modes of wave-chaotic dielectric resonators. In: E.Wolf (Ed.), Progress in Optics. Elsevier, pp. 75–137. https://doi.org/10.1016/S0079-6638(05)47002-X.
[39] K. Korthout, P. F. Smet, and D. Poelman, "Whispering gallery modes in micron-sized SrS:Eu octahedrons," Appl. Phys. Lett., vol. 94, 2009, Art no. 051104, https://doi.org/10.1063/1.3078398.
[40] A. W. Poon, F. Courvoisier, and R. K. Chang, "Multimode resonances in square-shaped optical microcavities," Opt. Lett., vol. 1926, pp. 632–634, 2001, https://doi.org/10.1364/ol.26.000632.
[41] M. Lebental, N. Djellali, C. Arnaud, et al., "Inferring periodic orbits from spectra of simply shaped microlasers," Phys. Rev. A, vol. 76, 2007, Art no. 023830, https://doi.org/10.1103/PhysRevA.76.023830.
[42] I. Braun, G. Ihlein, F. Laeri, et al., 2000. Hexagonal microlasers based on organic dyes in nanoporous crystals. Appl. Phys. B 70, 335–343. https://doi.org/10.1007/s003400005005.
[43] A. Bäcker, R. Ketzmerick, S. Löck, et al., "Dynamical tunneling in mushroom billiards," Phys. Rev. Lett.Art no, vol. 100174103, 2008, https://doi.org/10.1103/PhysRevLett.100.174103.
[44] T. J. Kippenberg, R. Holzwarth, S. A. Diddams, 2011. Microresonator-based optical frequency combs. Science 332, 555. https://doi.org/10.1126/science.1193968.
[45] S.-X. Qian, J. B. Snow, H.-M. Tzeng, R. K. Chang, 1986. Lasing droplets: highlighting the liquid-air interface by laser emission. Science 231, 486. https://doi.org/10.1126/science.231.4737.486.
[46] V. M. Apalkov and M. E. Raikh, "Directional emission from a microdisk resonator with a linear defect," Phys. Rev. BArt no, vol. 70195317, 2004, https://doi.org/10.1103/PhysRevB.70.195317.
[47] M. Hentschel and K. Richter, "Quantum chaos in optical systems: The annular billiard," Phys. Rev. E, vol. 66, 2002, Art no. 056207, https://doi.org/10.1103/PhysRevE.66.056207.
[48] R. Bekenstein, Y. Kabessa, Y. Sharabi, et al., 2017. Control of light by curved space in nanophotonic structures. Nat. Photon. 11, 664–670. https://doi.org/10.1038/s41566-017-0008-0.
[49] V. H. SchultheissS. Batz, A. Szameit, et al., "Optics in curved space," Phys. Rev. Lett., vol. 105, 2010, Art no. 143901, https://doi.org/10.1103/PhysRevLett.105.143901.
[50] R. Bekenstein, J. Nemirovsky, I.Kaminer, and M. Segev, "Shape-preserving accelerating electromagnetic wave packets in curved space," Phys. Rev. X, vol. 4, 2014, Art no. 011038, https://doi.org/10.1103/PhysRevX.4.011038.
[51] D. Wang, C. Liu, H. Liu, J. Han, S. Zhang, 2018. Wave dynamics on toroidal surface. Opt. Express 26, 17820–17829. https://doi.org/10.1364/OE.26.017820.
[52] D. A. Genov, S. Zhang, X. Zhang, 2009. Mimicking celestial mechanics in metamaterials. Nat. Phys. 5, 687–692. https://doi.org/10.1038/nphys1338.

Supplementary Material: The online version of this article offers supplementary material (https://doi.org/10.1515/nanoph_2020-0083).